

CFD ANALYSES OF MAIN FLOW PENETRATION DEPTH IN ISOLATED BRANCH LINES

Brandon LaFleur, Victor Petrov, and Annalisa Manera

Department of Nuclear Engineering and Radiological Sciences, University of Michigan,
2355 Bonisteel Boulevard, Ann Arbor, MI 48109-2104, USA
blafleur@umich.edu; petrov@umich.edu; manera@umich.edu

ABSTRACT

Thermal fatigue has been identified as a mechanism that can potentially lead to wall cracking in dead-end piping branching from the reactor primary coolant piping. This phenomenon can take place in LWRs, as well as advanced reactors cooled by salts or liquid metals. The main flow stream (hot) creates a secondary flow swirl which propagates in the stagnant branch line (cold). In the side branch, stratification occurs below the flow swirl, where also transition from turbulent to laminar flow occurs. The hot flow swirl interacts with the stratified layer present in the colder branch line, leading to fluctuations of the thermally stratified front which consequently induces thermal fatigue on the branch line walls.

The penetration depth and frequencies of the temperature oscillations depend on the main flow velocity, system geometry, and temperature difference between the fluid in the main pipe, and the branching line. This study seeks to simulate this phenomenon and compare to experimental results. Experimental data have shown that three distinct regions exist in the branch line flow, and experimental correlations have been found relating the flow swirl penetration depth to the main pipeline velocity. In this study, the flow patterns developing in the branch lines are investigated for pipes of three different sizes.

Flow structures in a closed branch pipe connected to a high velocity flow in main pipe were simulated using the standard $k-\epsilon$ two layer model in STAR-CCM+. The vorticity decay in the closed branch pipe was used to determine the boundaries of the first flow region. The decay of tangential velocity was used to determine the flow swirl penetration depth. The results were compared to experimental data for three geometries characterized by different branch pipe length and diameter. The experimental trends were successfully captured with CFD simulations.

KEYWORDS

Branch lines, thermal fatigue, penetration depth, vorticity decay, experimental validation, CFD

1. INTRODUCTION

Thermal fatigue has been identified as a mechanism that can potentially lead to wall cracking in dead-end piping branching from the reactor primary coolant piping. This phenomenon can take place in LWRs, as well as advanced reactors cooled by salts or liquid metals, and the involved phenomena are very different from the ones responsible for thermal fatigue in T-junctions. Thermal fatigue in stagnant branch lines departing from hot or cold legs of PWRs is of high interest to the nuclear industry, as the current screening criteria developed by EPRI[1] are overly conservative and hundreds of branch lines need to be periodically monitored at plant outages in the US. In addition, in the past 15 months 10 events have been registered at US plants, of which 2 involved mixing tees and 8 involved branch lines.

In stagnant branch lines, the main (hot) flow from the main pipe (e.g cold or hot leg of a PWR) creates a secondary flow swirl which propagates in the stagnant branch line (cold). In the side branch, stratification

occurs below the flow swirl, where transition from turbulent to laminar flow also occurs. The hot flow swirl interacts with the stratified layer present in the colder branch line, leading to fluctuations of the thermally stratified front which consequently induces thermal fatigue on the branch line walls. The phenomenon is illustrated in Figure 1

While thermal-fatigue in T-junctions has been investigated in depth and the phenomena are well understood, more research efforts are still needed with regards to thermal fatigue in branch lines. Predicting thermal cycling in stagnant branch lines by means of analytical/empirical models has historically proven to be challenging, due to the complex nature of the fluid dynamics interactions (EPRI[1]). At the same time, the assessment of the predictive capabilities of high fidelity computational fluid dynamics (CFD) methodologies (such as Large Eddy Simulations) has been hindered by the lack of sufficiently detailed experimental data, which do exist for thermal fatigue in T-junctions instead.

Because of the difference in turbulence phenomena, validation of CFD RANS and LES methodologies on T-junction experiments such as the OECD/NEA Vattenfall international benchmark (Mahaffy and Smith, 2010[2,3]; see also Figure 2) cannot give confidence on the applicability of similar methodologies to investigate thermal fatigue in branch lines. This is because, while in T-junctions turbulence is mostly generated in the main pipe downstream the T-junction where the hot and cold stream meet, in branch lines turbulence is transported in the side branch by a flow swirl generated at the interface between high fluid velocity (main pipe) and stagnant water (branch line).

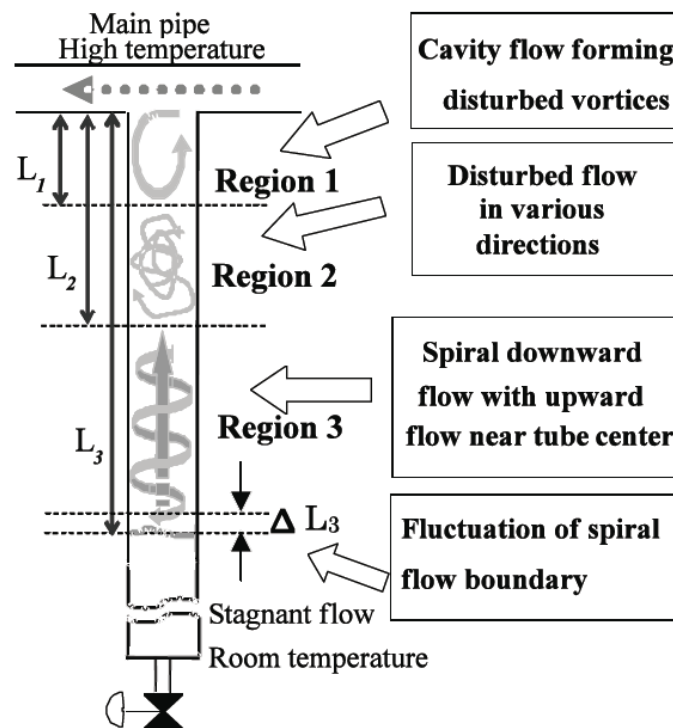


Figure 1. Flow regions in a vertical branch pipe [4].

The aim of this paper is to assess the capabilities of current RANS steady-state models to predict the extent of swirl penetration into a stagnant dead end branch pipe. RANS models could potentially be used

to design forthcoming experiments, define pipe screening criteria or to obtain initial flow fields for LES models.

2. DESCRIPTION OF THE EXPERIMENTAL SET UP

Experiments published by T. Iguchi et al.[4] have been selected for the validation of steady-state RANS models. A scheme of the experimental facility is presented in figure 2. The maximum flow velocity in the main pipe is limited to 15 m/s. The experimental loop includes a heat exchanger which allows temperature differences between main and branch lines flows of up to 50 degree. However in the present paper only the adiabatic cases were modeled. The test section is made out of transparent acrylic with a branch line diameters D_b listed in Table I and a rectangular main pipe with dimensions of 60mm x 10mm (WxH) as indicated in figure 3. Even though the actual reactor main pipe has a round shape, and the diameter might vary between 700mm-800mm depending on the actual plant design, it is next to impossible to use actual main pipe dimensions in a lab setup due to the enormous flow rate required to obtain realistic main pipe flow velocities. The experimentalists had therefore opted for a rectangular main pipe cross-section. Although flow through a rectangular pipe would produce secondary flows in the corners, it is judged that this would not affect the behavior of the penetration depth. The penetration depth is assumed to be driven mainly by the flow at the direct interface between the branch and main pipe. The flow was traced using formed polystyrene particles and recorded by a video camera [5].

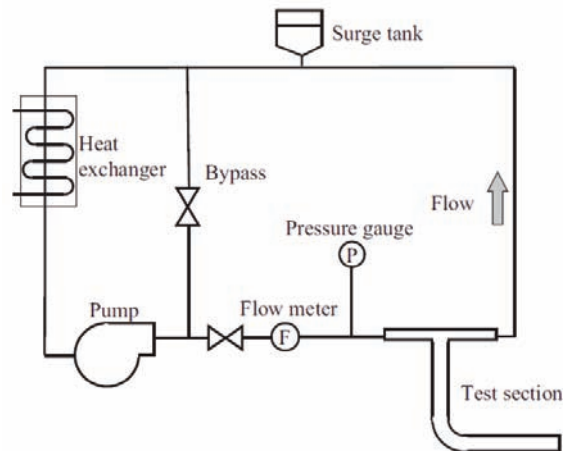


Figure 2. Scheme of the experimental set-up [5].

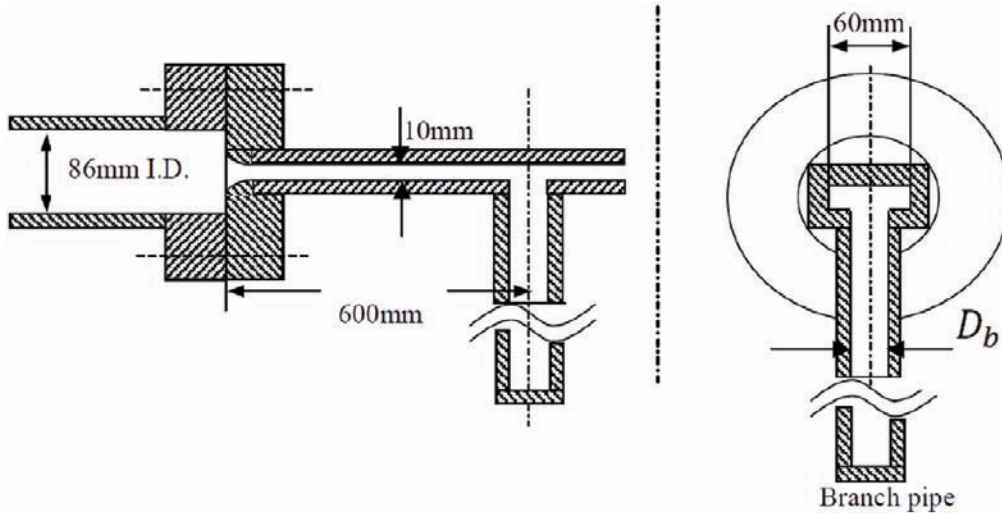


Figure 3. Cross sections of main pipe and branch line in the experimental set-up [4].

Table I. Pipe size

| Nominal Size | Inner Diameter [mm] |
|--------------|---------------------|
| JIS 2B | 43 |
| JIS 3/2B | 34 |
| JIS 1B | 21 |
| JIS 3/4B | 16 |
| JIS 1/2B | 12 |
| JIS 1/4B | 8 |

According to experimental observations, the flow patterns in the straight branch line were divided into three main regions, as indicated in figure 1 [4]. Region 1 is characterized by a vertical vortex induced right below the main line that penetrates roughly a third of the total penetration depth. In Region 2 random fluctuations were observed, where no clear flow pattern could be identified. Region 3 is characterized by a spiral peripheral flow and upwards central flow. At the end of this region, a stratified layer is present (see label ΔL_3 in Figure 1) and with high probability is responsible for the occurrence of thermal fatigue in branch lines observed in operating plants. Although the hot water rarely penetrates to this depth, the turbulent swirl penetration induced an oscillation of the stratified layer which might ultimately lead to thermal fatigue of the branch line wall.

3. CFD MODEL

The experimental facility shown in Figure 2 was modeled using the commercial CFD code STAR-CCM+ [6]. The CFD model is reported in figure 4.



Figure 4. Modeling scheme.

The flow development region in the experimental set-up is $35D_h$ long, therefore the flow in the main line can be assumed to be fully developed. All simulations discussed in the following sections were performed using the standard $k - \varepsilon$ turbulence model [7,8] combined with the two layer approach [9]. Future studies should aim to determine if a more applicable model exists to capture this phenomena. Some computational studies currently reported in the literature involve more computational intensive simulations that take into account anisotropy in the turbulence. However, the current simpler two equation model used for this study is shown to give promising results for swirl penetration in a dead end branch pipe.

3.1. Mesh Convergence Study

Before proceeding with the comparison with experimental data, it must be first ensured that the cells size used for the CFD model is appropriate to capture all relevant effects observed in the branch line flow. Therefore a detailed mesh sensitivity study has been carried out. The sensitivity study was performed at a mean flow velocity of 10 m/s in the main pipe and using the smallest branch pipe size JIS 1B. It is reasonable to assume that larger branch pipes would not need a finer mesh than the JIS 1B model. The mesh convergence study was systematically carried out as follows: the Model was divided into three free parts, the round tube inlet, the square pipe section (termed the "sleeve") and the T-junction respectively. As there are many features in the model that required special attention during meshing, the problem was broken up into four smaller problems. First, a converging study for tube mesh was carried out; this was also used to get a fully developed inlet velocity profile for the complete model. Second, a converged mesh for an isolated sleeve was obtained. Third, a model which combined the round tube with a portion of the sleeve was considered. An additional study was performed using locally refined mesh at the intersection of the different parts. This last step is needed because there are complex 3-D flows happening in areas of intersection of round and square pipes which require a finer mesh to capture. Finally, a mesh convergence study was performed for the intersection region between the sleeve and the branch pipe. The mesh convergence was assessed by comparing velocity profiles obtained for the same region with different mesh resolutions.

The convergence of the inlet tube velocity profile convergence is shown in figure 5(a). In figure 5(b) the maximum local deviation in the velocity profile is presented. This never exceeds 1% for the selected cells size range. As a result of this first convergence study, a mesh with cell size of 0.002m with 2 prism layers and a prism layer thickness of $3E-4$ m was selected for further simulations.

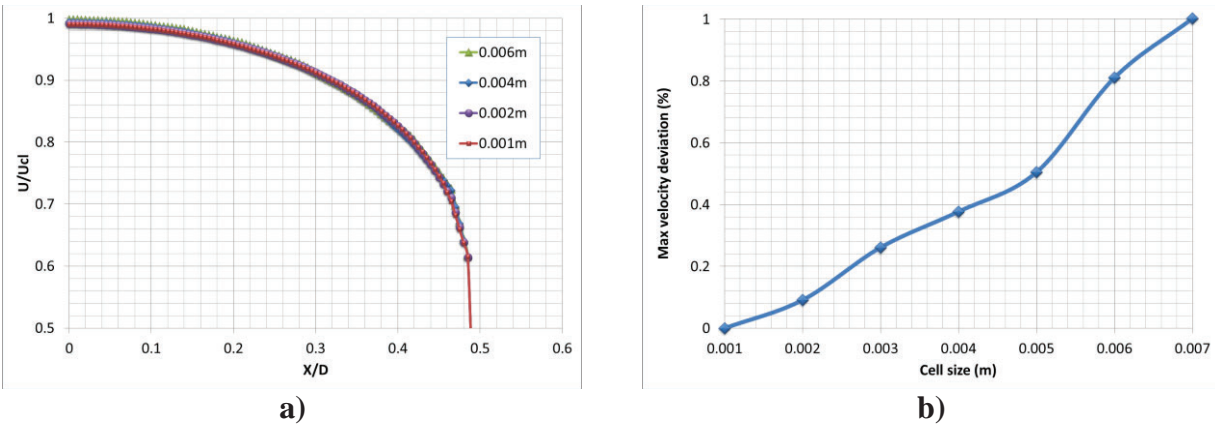


Figure 5. Round tube velocity convergence.

The velocity profiles obtained in the rectangular pipe section with a different mesh base size and the prism layer thickness of 0.00035m are shown in figure 6. The velocity profile in the proximity of the wall region is very important for this section, since this will significantly affect the penetration depth in the branch line. A base size of 0.001m is deemed sufficient for the model.

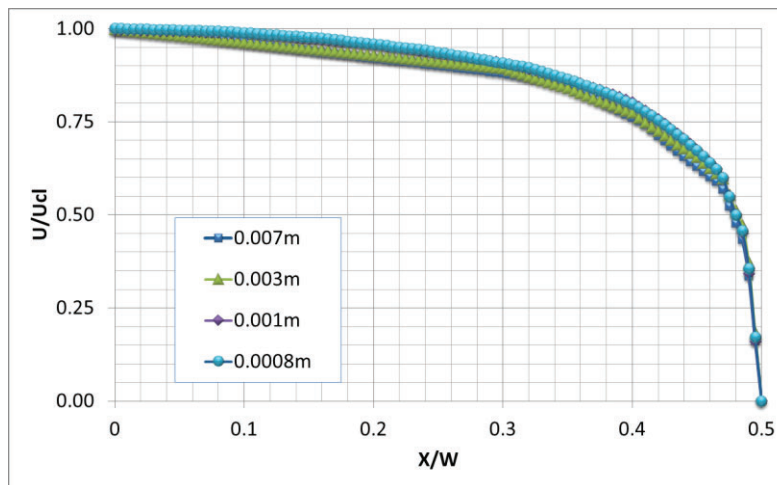


Figure 6. Rectangular pipe velocity convergence.

Extra local mesh refinement was applied at the intersection region between the round tube and the rectangular pipe, as indicated in figure 7 (left). According to the figure 7 (right), the mesh refinement has a minor overall effect on the velocity profile but serves for smoother transition between regions and reduces the risk of numerical instabilities at sharp edges. Given these considerations, the final model for the intersection region was refined with a 0.0008m cell size, with no adjustments to the prism layer.

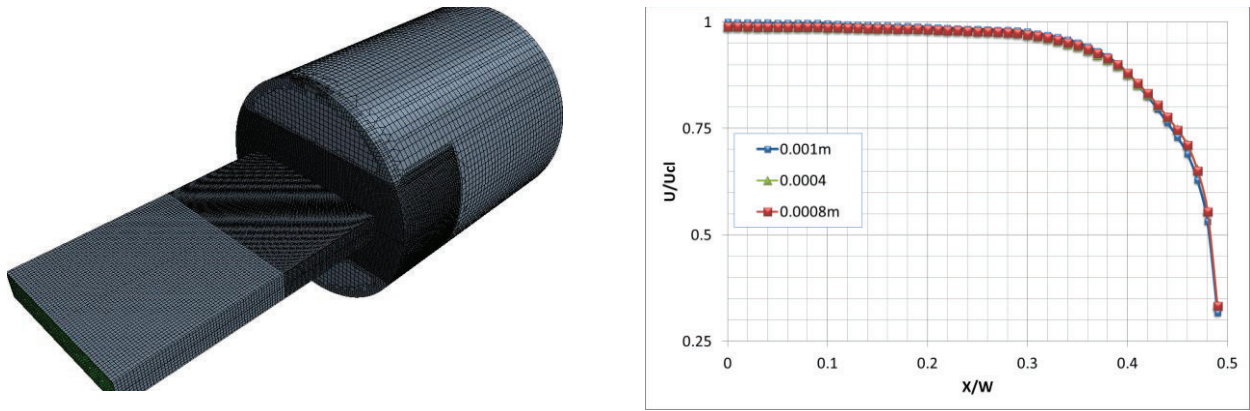


Figure 7. Intersection region mesh (left) and velocity profile in rectangular section (right).

The mesh convergence for the T-Junction section was performed applying a local mesh refinement to the region which covers the intersection between main pipe and branch line, including a considerable length downstream the branch pipe. The mesh convergence was assessed by comparing the velocity profile along the branch pipe central axis. The mesh region and the branch line axial velocity profiles are shown in figure 8 (left) and 8 (right) respectively. Close to the inlet of the branch line, the velocity profiles are practically identical. Slight differences are observed at the depth of around 0.2 branch pipe length, where the transition from region 1 to region 2 occurs (see figure 1). The velocity at this location gives an estimation for the vortex size. But smaller distance between picks for cells size of 0.0004m and cells size of 0.0008m rather than between cells size of 0.0008m and cells size of 0.001m could be also considered as an evidence of convergence. Velocity oscillations at the depth below 15D have very low magnitude and are practically very difficult to resolve with RANS models.

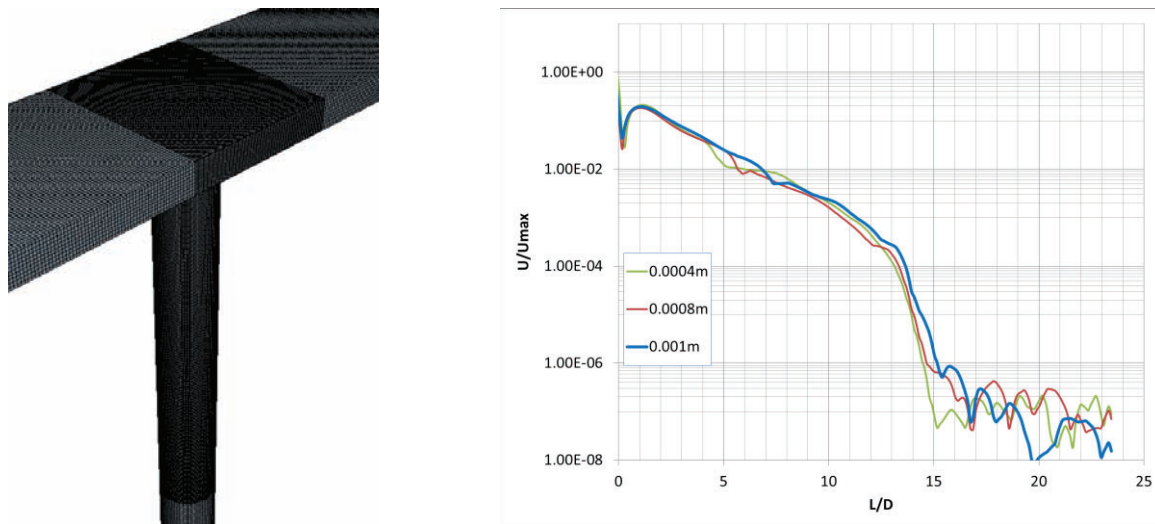


Figure 8. T-Junction region mesh (left) and branch pipe velocity profile (right).

Based on the above mesh sensitivity study, values of cell sizes and prismatic layers were selected for each mesh region, as summarized it Table II.

Table II. Finalized mesh

| Mesh region | Base Size (m) | Prism Layer Thickness (m) | Number of prisms | y+ |
|-----------------|---------------|---------------------------|------------------|---------|
| Round Tube | 0.002 | 0.003 | 2 | 43 |
| Sleeve | 0.001 | 0.00035 | 2 | 33 |
| Tube and Sleeve | 0.0008 | 0.00035 | 2 | 0.5-110 |
| T-junction | 0.0008 | 0.00035 | 2 | 0.1-40 |

To reduce the computational costs, the whole model up to the T-Junction was simulated to gather flow profiles at the inlet of the T-Junction for various flow velocities. These were then employed to model different branch pipe diameters.

3.2. Simulation Results

The following list of branch pipe diameters was investigated: JIS 1B, JIS 3/2B, and JIS 2B (see Table I). This provided ample material to validate the techniques used to determine L_1 and L_2 defined in Figure 1. A visualization of the stream lines obtained for the JIS 1B simulation is reported in Figure 9. It can be seen that the general flow structures observed in the experiments [5] are correctly captured by the steady-state CFD RANS simulations. This includes the vortex in region 1 that rotates with the direction of main flow, and the outward spiral with an upward flow in the tube center for region 3. As for the experiments, region 2 is not clearly defined.

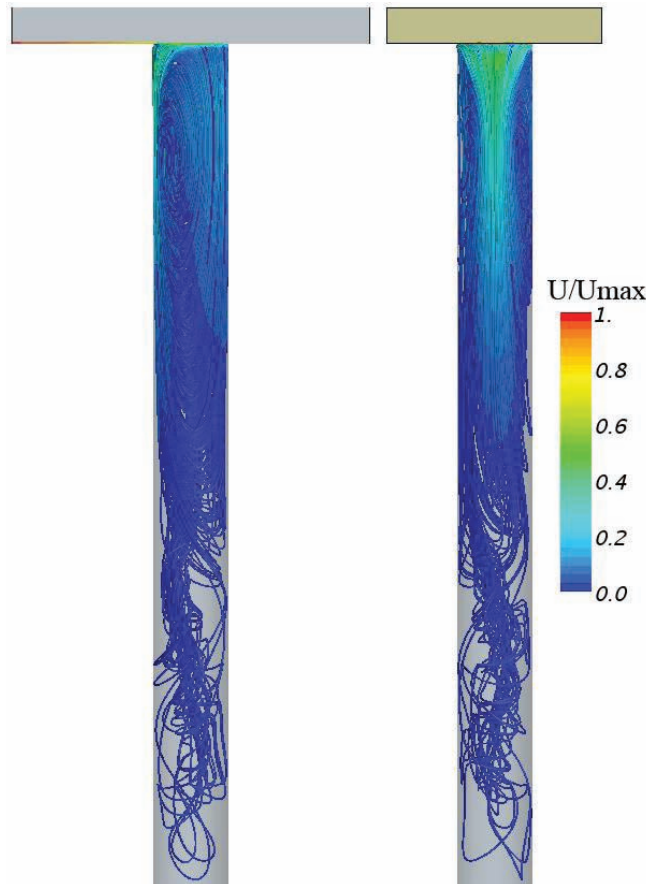


Figure 9. Flow streamlines front view (left) and side view (right).

To determine where L_1 ends, the vorticity decay shown in figure 10 is used. In the y-direction (the direction perpendicular to the main flow direction and branch pipe) this magnitude will have its highest values where there are high amounts of rotation in the flow. By finding where this value drops below 1% of its maximum value, the L_1 length can be univocally identified. It is illustrative to note that no matter the flow velocity of the main pipe, all vorticity decay plots show that they intersect the zero vorticity line at about the same point. Note that this point gives a dimensionless relationship of L_1/D of about 3, as was observed in the experimental results [4]. To determine the L_3 cutoff, or the swirl penetration depth, the decay of the tangential velocity is used, as the magnitude of the tangential velocity is indicative of the region where the flow structure is still present. The average tangential velocity is presented in figure 11 for the different branch pipe diameters.

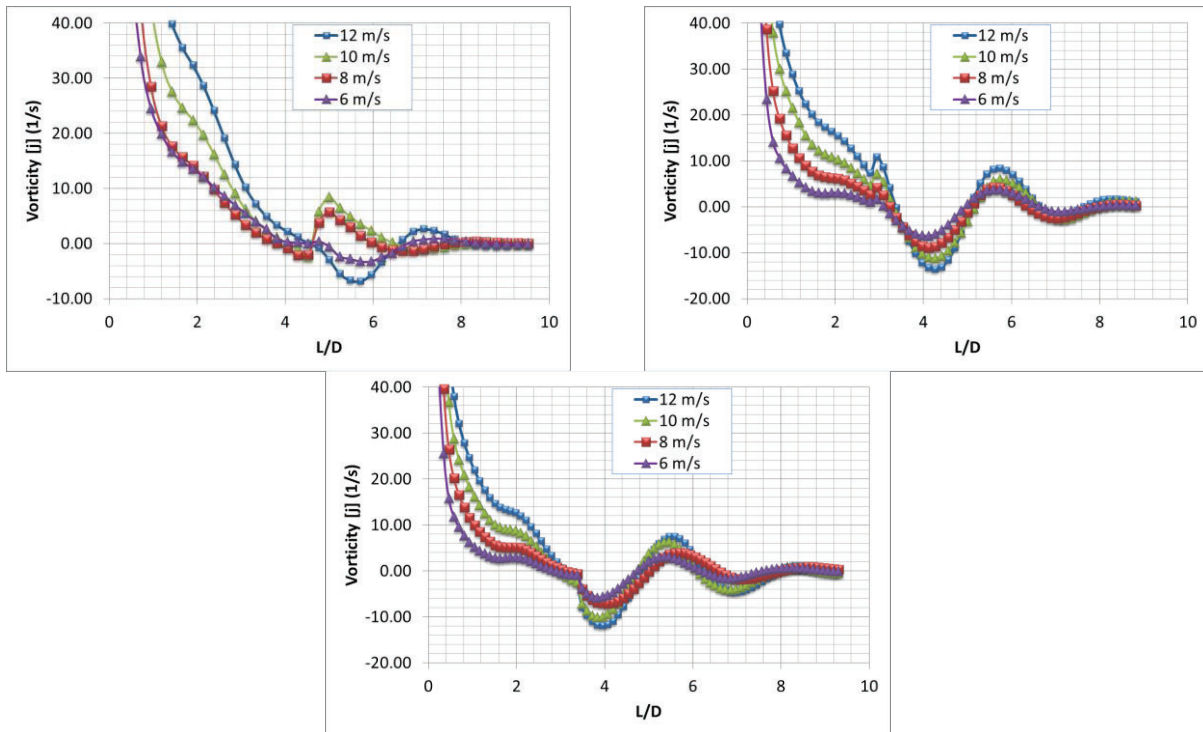


Figure 10. Average vorticity in the y direction along branch for JIS 1B (left), JIS 3/2B(right) and JIS 2B (bottom).

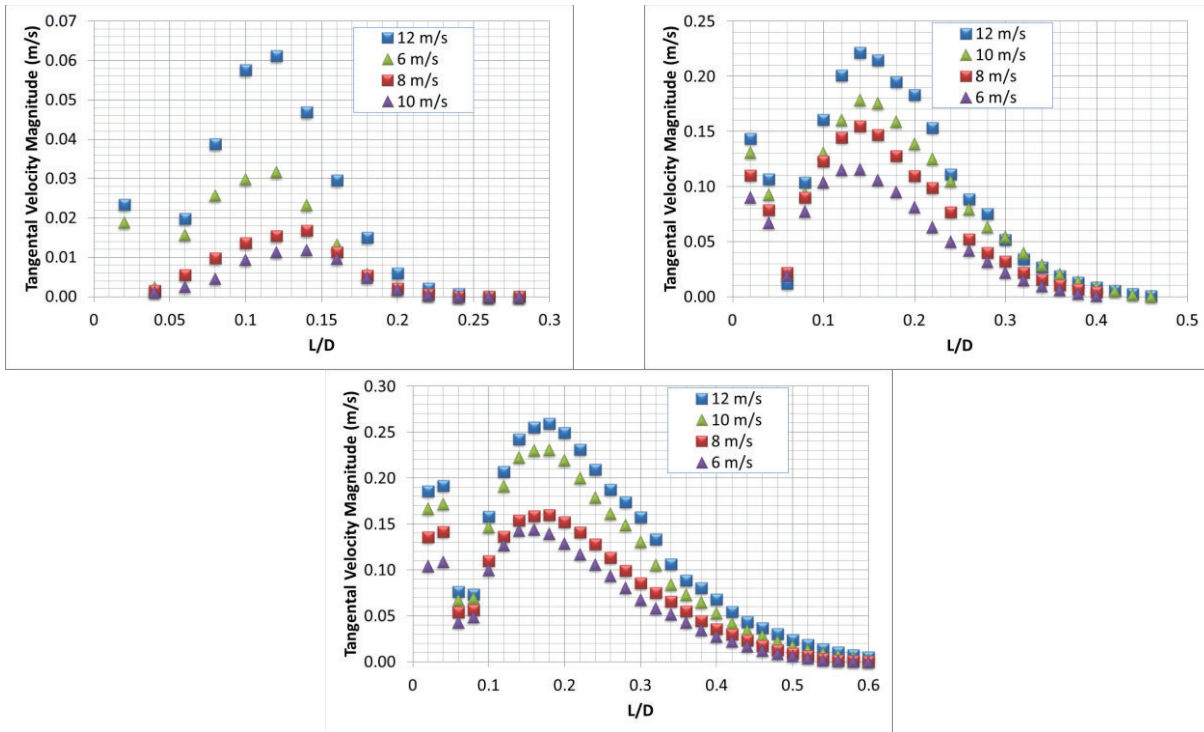


Figure 11. Average tangent velocity magnitude along branch for JIS 1B (left), JIS 3/2B(right) and JIS 2B (bottom).

To compare simulation results directly to the reported experimental data, dimensionless relationships are used. Figure 12 (left) shows the ratio between L_1 and the pipe diameter for both simulation and experiment as a function of flow velocity. As it was already mentioned above, no matter the pipe length or flow velocity, for both simulation and experiment, this dimensionless value lands at a value of about 3. Dimensionless results for L_3 and pipe diameter as a function of flow velocity are indicated in figure 12 (right). Here the general experimental trend is matched by the simulations. As a matter of fact, most of the experimental data points are in close proximity to the simulation results with the exception of the JIS 3/2B data point corresponding to a flow velocity of 12 m/s.

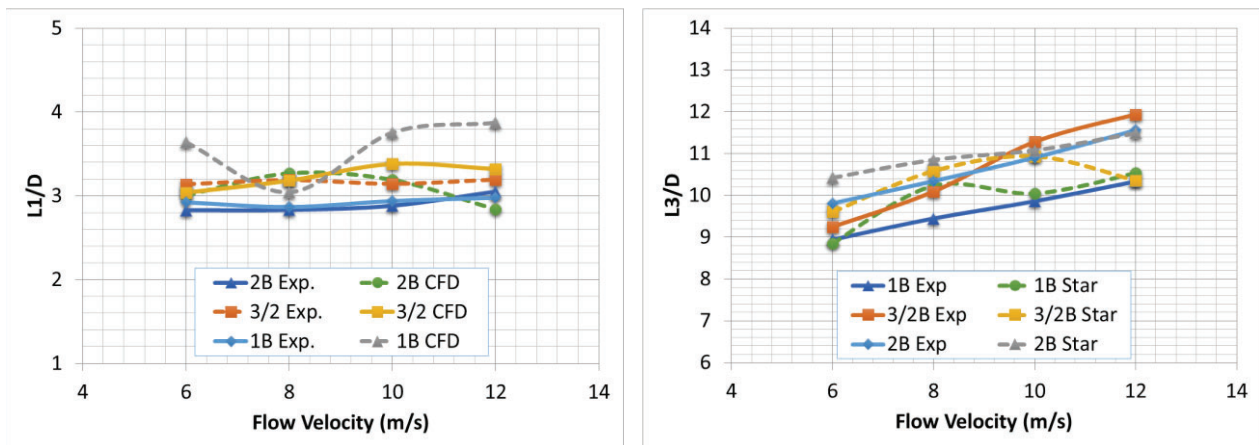


Figure 12. Dimensionless relationship between L_1 and pipe diameter (left) and L_2 and pipe diameter (right).

Figure 13 shows a correlation suggested by [4] for experimental (left) and corresponding simulation results (right), whose relationship is given in equation (1), and relates the Reynolds number to the dimensionless penetration depth. Good agreement is seen here as well.

$$\frac{L_3}{D} = 0.21Re^{0.31} \quad (1)$$

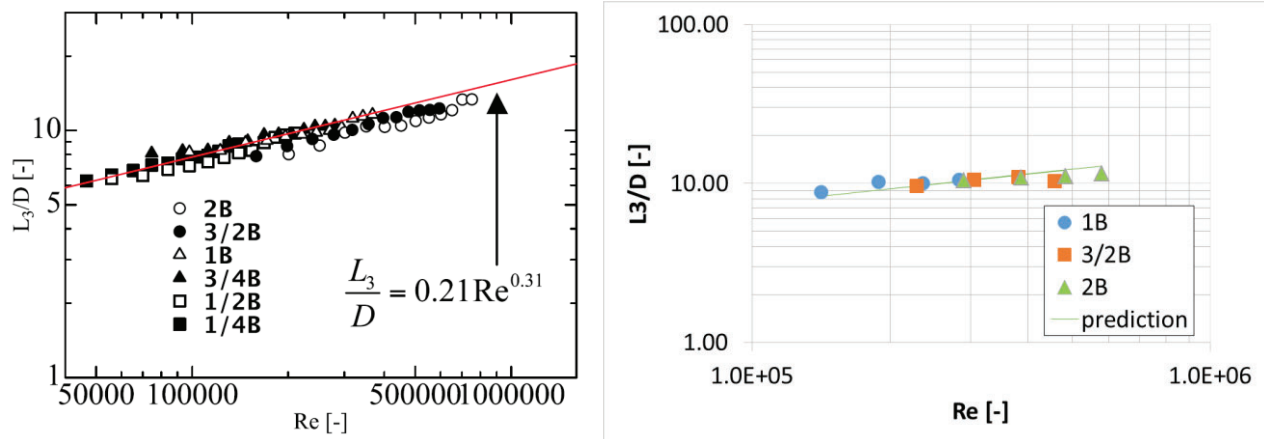


Figure 13. Dimensionless relationship between Reynolds number and L_3 , experiment (left) simulation (right).

4. CONCLUSIONS

In the present study, experimental data available in the open literature have been used to demonstrate the capability of RANS steady-state models to predict the penetration depth in branch lines. Computational studies were successfully performed for three branch line diameters and a very good qualitative as well as quantitative agreement with experiment data was found. This result is particularly significant, considering that all computational studies currently reported in the literature involve much more computational intensive unsteady RANS or Large Eddy Simulations. Future investigations will be focused on assessing the importance of turbulence anisotropy.

REFERENCES

1. Materials Reliability Program Interim Report on Thermal Cycling Model Development for Representative Un-isolable Piping Configurations (MRP-81), EPRI, Palo Alto, CA, and U.S. Department of Energy, Washington, DC: 2002. 1003527.
2. Mahaffy, J. H., Smith, B. L., 2010. OECD/NEA Vattenfall - synthesis of benchmark results. Experimental Validation and Application of CFD and CMFD Codes to Nuclear Reactor Safety Issues (CFD4NRS-3), Bethesda, MD, September 14 - 16.
3. OECD/NEA, (2011). "Report of the OECD-NEA-Vattenfall T-Junction Benchmark exercise", Report NEA/CSNI/R(2011)5, 12 May, 2011.
4. T. Iguchi, A. Saito, N. Takenaka, K. Miyoshi, A. Nakamura, "Experimental Study on Penetration length in a Small Size Branch Pipe In A Nuclear Power Plant", *14th International Topical meeting on Nuclear Reactor Thermal hydraulics (NURETH14-178)*, September 25-30, 2011.
5. A. Nakamura, K. Miyoshi, T. Oumaya, N. Takenaka, S. Hosokawa, D. Hamatani, M. Hase, D. Onojima, Y. Yamamoto, A. Saito, Temperature fluctuation phenomena in a normally stagnant pipe

connected downward to a high velocity and high temperature main pipe. *Nucl. Eng. Des.*, **269** (2014), pp. 360–373

6. STAR-CCM+ User Guide, v9.02, CD-adapco 2014.
7. Jones, W.P., and Launder, B.E. 1972. “The Prediction of Laminarization with a Two-Equation Model of Turbulence”, *Int. J. Heat and Mass Transfer*, **15**, pp. 301-314.
8. Launder, B.E., and Sharma, B.I. 1974. “Application of the Energy Dissipation Model of Turbulence to the Calculation of Flow Near a Spinning Disc”, *Letter in Heat and Mass Transfer*, vol. **1**, no. 2, pp 131-138.
9. Rodi, W. 1991. “Experience with Two-Layer Models Combining the k-e Model with a One-Equation Model Near the Wall”, *29th Aerospace Sciences Meeting*, January 7-10, Reno, NV, AIAA 91-0216.